Supplementary Information

Bifunctional rhenium-copper nanostructures for intensified and stable ethanol synthesis via hydrogenation of dimethyl oxalate

Zhongnan Du, ‡ [a] Meng Chen, ‡ [b] Xuepeng Wang,[a] Xingkun Chen,*[a] Xiaoling Mou,[a] Yuan Tan,[a] Wenshao Yang,[a] Chuanqi Huang,[a] Hejun Zhu,[b] Ronghe Lin*[a] and Yunjie Ding*[a,b,c]

[a.] *Hangzhou Institute of Advanced studies, Zhejiang Normal University, 1108 Gengwen Road, Hangzhou 311231, China.*

[b.] *Dalian National Laboratory for Clean Energy, Dalian Institute of Chemical Physics, Chinese Academy of Sciences, 457 Zhongshan Road, Dalian 116023, China.*

[c.] *The State Key Laboratory of Catalysis, Dalian Institute of Chemical Physics, Chinese Academy of Sciences, 457 Zhongshan Road, Dalian 116023, China.*

‡ Equal contribution

* Corresponding authors. E-mails: dyj@dicp.ac.cn, cxklned@zjnu.cn, catalysis.lin@zjnu.edu.cn

Catalyst synthesis

The Cu/SiO_2 catalyst (nominal metal content 20 wt.%) was prepared using the ammonia evaporation (AE) method as previously described.[1] In a typical synthesis, 12.6 cm^3 ammonia solution (25-28 wt.% NH_4OH, Sinopharm company) was mixed with 70 cm^3 0.3 M copper nitrate solution (($Cu(NO_3)_2$•$3H_2O$, >99.0 wt.%, Sinopharm company) and stirred for 5 min. The pH of the complex was about 11. Then 11.52 g-fumed silica (SiO_2, AEROSIL 300) was added to the copper ammonia complex solution and the mixture was stirred at 308 K for another 4 h. After this, the suspension was heated to 363 K to evaporate the ammonia until the pH decreased to 6-7. The solid was filtered, washed with 500 cm^3 of deionized water, dried at 393 K for 10 h, and calcined in air at 823 K (4 h, ramping rate 1 K min^{-1}). The bimetallic $Re-Cu/SiO_2$ catalysts were prepared by an incipient wetness impregnation method. Typically, the as-prepared Cu/SiO_2 catalyst was impregnated with an aqueous solution of NH_4ReO_4 (99.99 wt.%) at room temperature. After was stayed at room temperature overnight, the solid was dried at 393 K for 10 h and calcined at 823 K (4 h, ramping rate 1 K min^{-1}). An additional Re/SiO_2 catalyst (nominal metal content 5 wt.%) was prepared following the same method but using the commercial SiO_2 (AEROSIL 300) as the support. Another bimetallic catalyst (Re_5-Cu_5/SiO_2-co) was prepared by a one-pot co-impregnation method, using $Cu(NO_3)_2$•$3H_2O$ and NH_4ReO_4 as the precursors and SiO_2 (AEROSIL 300) as the carrier. The thermal activation of the catalyst was following the same protocol for the previous $Re-Cu/SiO_2$ catalysts.

Catalyst characterization

The contents of Cu and Re in the catalysts were determined by an inductively coupled plasma optical emission spectrometer (ICP-OES, PerkinElmer, and Optima 7300 DV). Nitrogen sorption was measured at 77K on a Quanta chrome NT3LX-2 instrument after degassing the samples at 673 K for 3 h. The specific surface area and the pore size distribution were calculated by the Brunauer-Emmett-Teller (BET) and the BJH methods, respectively. Fourier-transform infrared (FT-IR) spectroscopy analysis was performed on a Bruker Tensor 27 FT-IR spectrometer using the KBr pellet method with the mass ratio of KBr to sample of 60. The spectra were collected in the range of 400–4000 cm^{-1} with 32 scans and a resolution of 2 cm^{-1} at room temperature. For *in situ* FT-IR with CO adsorption, the spectra were recorded on a Nicolet iS50 spectrometer with a spectral resolution of 2 cm^{-1}. Self-supporting pellets were prepared from the sample powder and treated directly in the IR cell. The purpose-made cell allowed the possibility of low-temperature experiments and was connected to a vacuum-adsorption apparatus. Prior to the adsorption measurements, the samples were first reduced by H_2 (503 K, 4 h) and evacuated for another 1 h at the same temperature. After cooling to 323K, the background spectrum A was collected. Then the sample was exposed to CO for 30 min and evacuated for another 1 h. The spectrum B was obtained under these conditions. The infrared spectrum of the sample adsorbing CO was obtained by deducting background (spectrum A) from spectrum B. X-ray diffraction (XRD) analysis was conducted on an X'Pert 3, PANalytical X-ray diffractometer using Cu Kα radiation in a scanning angle (2θ) range of 10-90° at a speed of 0.2° min^{-1}. The tube voltage and the current were 40 kV and 40 mA, respectively. For *in situ* XRD, the catalyst precursor was placed in a reaction cell manufactured by Anton Parr (XRK 900). H_2 was introduced at a flow rate of 30 cm^3 min^{-1}, and the temperature ramping programs were performed from room temperature to 873 K with a heating rate of 5 K min^{-1}. The XRD patterns were collected after sample temperature reached the

preset temperatures for 10 min. The crystallite size of Cu nanoparticles was calculated by Scherrer equation using the Cu (111) facet at 43.2° 2θ following Eq. (1):

$$D = \frac{k\lambda}{Bcos\theta} \qquad Eq.(1)$$

where, k is the Scherrer constant (0.89), λ is the wavelength of X-ray (0.154056 nm), B is the Full Wave at full width at half maximum of diffraction peak, and θ is the diffraction angle. Hydrogen temperature-programmed reduction (H_2-TPR) was studied on a Micromeritics Autochem II 2920 chemisorber equipped with a thermal conductivity detector. For H_2-TPR, the sample (150 mg) was pretreated in a quartz U-tube reactor with a He gas stream (30 cm^3 min^{-1}) at 473 K for 1 h. After cooling to room temperature, a 10% H_2/Ar flow (50 cm^3 min^{-1}) was introduced and the sample was heated to 1073 K (10 K min^{-1}). The surface topography images of the sample were obtained by Talor S-FEG Field emission transmission electron microscope (TEM). The sample powder was dispersed in ethanol by ultrasonication and then the specimen was obtained by dropping a droplet suspension on a carbon film supported on a copper grid for TEM analysis. High-angle annular-dark-field scanning transmission electron microscopy (HAADF-STEM, JEOL JEM-ARM200F). X-ray photoelectron spectroscopy (XPS) and the X-ray Excited Auger electron spectroscopy (XAES) analysis of the catalysts were carried out on a Thermo ESCALAB 250Xi spectrometer using a 15 kV Al Kα X-ray source as a radiation source. The binding energy was calibrated using the C 1*s* peak (284.6 eV) as the reference.

Catalytic test

The catalytic vapor-phase hydrogenation of DMO was performed in a micro-reaction system over a stainless steel fixed-bed reactor (inner diameter, 10.0 mm; length, 660 mm), equipped with a thermocouple and a mass flow controller for the control of reaction temperature and hydrogen flow rate. Typically, 1.0 g of the catalyst was placed in the center of the reactor, and reduced *in situ* with H_2 (30 cm^3 min^{-1}, 503 K, 3 bar, 4 h). After cooling to the reaction temperature, the system pressure was increased to 15 bar with a back-pressure regulator. Then, a DMO solution (20 wt.% DMO in methanol, 99%, Analytic Reagent) was admitted using a plunger pump (NP-KX-210, Nihon seimitsu kagaku co., ltd). The weight liquid hourly space velocity based on DMO (WLHSV(DMO)) was in the range of 0-3.5 h^{-1}. The reaction products were collected by a cold trap kept at 278 K with cooling water and analyzed offline with an Agilent 7890B chromatograph equipped with an HP-FFAP capillary column (30 m×0.32 mm×0.25 μm) and a flame ionization detector (FID) using *n*-butanol as the internal standard. For product identification, the reaction effluents were also analyzed offline with an Agilent 7890B chromatograph coupled with mass spectrometer (Agilent 5977B MSD). The exhaust gas was analyzed and methane was not detected.

Table S1. Comparison of catalyst performance in DMO hydrogenation to ethanol.

Catalyst	Test conditions				Performance			Synthesis	Note	Ref.
	T / K	*P* / MPa	WLHSV / h^{-1}	H_2/DMO	Stability / h	X_{DMO} / %	S_{EtOH} / %			
Re-Cu/SiO_2	503	1.5	0.36	280	150	100	90	Ammonium evaporation and impregnation	5 wt.% Cu, 5 wt.% Re, DMO → MG → MA → ethanol	This work
Re-Cu/SiO_2	503	1.5	0.36	280	800	100	90	Ammonium evaporation and impregnation	20 wt.% Cu, 5 wt.% Re, DMO → MG → MA → ethanol	This work
β-Mo_2C/SiO_2	473	2.5	0.2	200	350	100	70	Hydrothermal synthesis, followed by H_2 reduction at 973 K	25 wt.% Mo_2C, DMO → MG → MA → ethanol	[2]
Cu-Mo_2C	473	2.5	0.2	200	300	100	67	Solid-state thermolysis at 1023 K in Ar	Cu/Mo molar ratio = 0.03, DMO → MG → MA → ethanol	[3]
Fe_2C_5	533	2.5	0.2	180	130	100	90	Precipitation followed by carbonization in a methanol-H_2 mixture	DMO → MG → MA → ethanol	[4]
Fe_2C_5+CuZnO-SiO_2	573	2.5	0.6	180	>110	100	~98	Fe_2C_5:precipitation followed by carbonization in a methanol-H_2 mixture. CuZnO-SiO_2: pydrolytic precipitation method.	Cu/Zn molar ratio = 9:1, DMO → MG → MA → ethanol	[5]
Cu/SiO_2	543	2	0.4	1840	-	100	88	Deposition precipitation	30 wt.%Cu, DMO → MG → EG → ethanol	[6]
B-Cu/SiO_2	553	2.5	2.0	200	100	-	86[a]	Ammonia evaporation hydrothermal and impregnation	19 wt.%Cu,1 wt.%B,	[7]
Ce-Cu/SiO_2	553	2.5	0.8	200	200	100	91.8	Urea-assisted gelation method	15.1 wt.% Cu, 1 wt.% Ce, DMO → MG → EG → ethanol	[8]
Ni-Cu/SiO_2	553	2.5	1.0	200	100	100	90	Ammonia evaporation	19.7 wt.% Cu, 1 wt.% Ni,	[9]

								hydrothermal and impregnation		
Cu-Al/SiO_2	553	2.5	0.2	200	40	100	95	Hydrothermal method	26 wt.% Cu, 1 wt.% Al,	[10]
ZnCu/MgO	513	2.5	0.257	200	200	100	98	One-pot sonochemical synthesis	56 wt.%Cu, 7 wt.% Zn,	[11]
Cu/B-CNTs	573	2.5	0.4	200	120	100	78.1	Sonication-assisted impregnation	14.5 wt.% Cu, DMO → MG → EG → ethanol	[12]
Cu/CNTs	573	2.5	0.4	200	120	99.8	46.4	Impregnation	15.3 wt.% Cu, DMO → MG → EG → ethanol	[12]
Cu/Al_2O_3	543	4.0	0.2	200	200	100	94.3	Surfactant-assisted synthesis	15 wt.% Cu, DMO → MG → EG → ethanol	[13]
Cu/ZrO_2/Al_2O_3	543	4.0	0.3	150	220	100	97.4	Co-precipitation method	40 wt.% Cu, DMO → MG → EG → ethanol	[14]
$MoNi_4$-MoO_x/Ni-foam	503	2.5	0.22	180	220	100	93	Hydrothermal synthesis and H_2 reduction at 673 K	DMO → MG → MA → ethanol	[15]
Cu@CuPSNT-in	553	2.5	2.0	200	300	100	85	Hydrothermal synthesis and impregnation	25 wt.% Cu, DMO → MG → EG → ethanol	[16]
Cu/RGO	513	2.5	0.26	200	n.a.	100	94	Sonochemical synthesis	45 wt.% Cu, DMO→MG → EG → ethanol	[17]
Cu/ZrO_2	493	2.4	1.0	80	120	100	93.1	Complexing and vacuum drying	Cu:Zr molar ratio = 45:55, DMO → MG → MA → ethanol	[18]
Cu/SiO_2	543	2.0	1.5	40	100	100	43.5	Deposition precipitation	20 wt.% Cu, DMO → MG → MA → ethanol	[19]
$FeNi_3$-FeO_x/Ni-foam	493	2.5	0.44	90	500	100	98	Hydrothermal synthesis and impregnation	DMO → MG → MA → ethanol	[20]

[a] Yield.

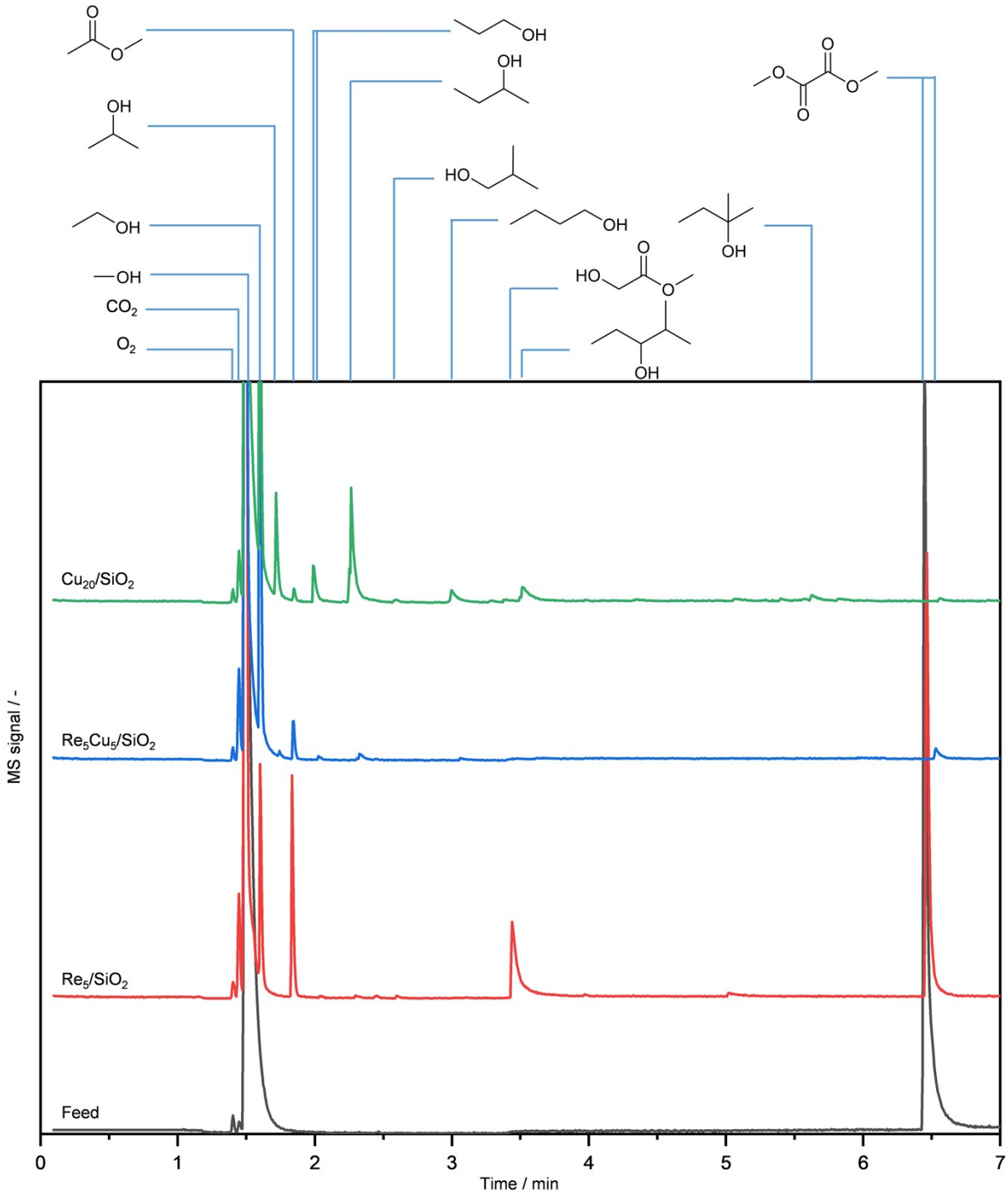

Fig. S1. GC-MS signals of the feed and liquid products of DMO hydrogenation over Re_5/SiO_2, Re_5Cu_5/SiO_2 and Cu_{20}/SiO_2 catalysts, accompanied with the product identification.

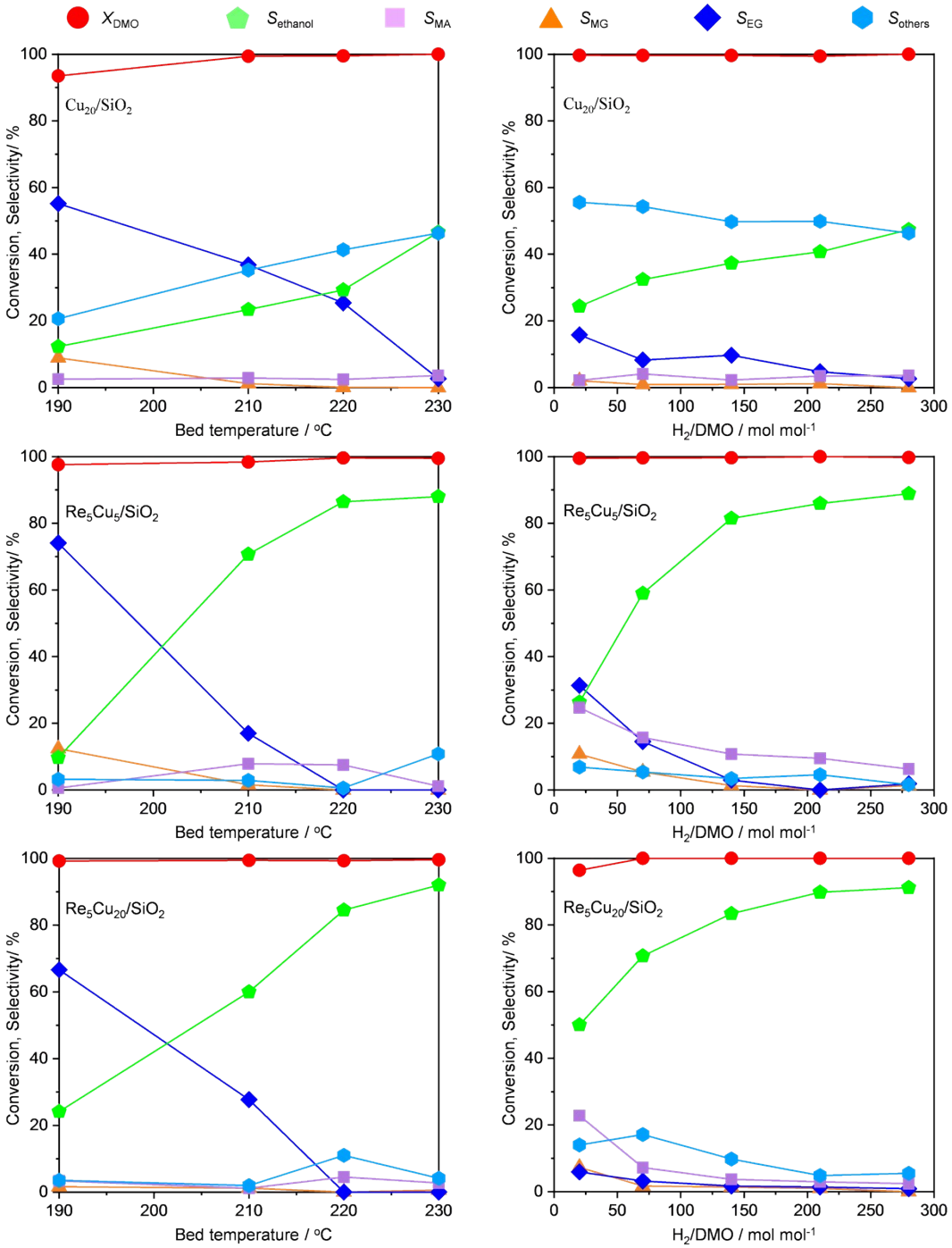

Fig. S2. Conversion and product selectivity as a function of the bed temperature (left: WLHSV(DMO)=0.36 h^{-1}, H_2/DMO=280, P = 15 bar) and the H_2/DMO ratio (right: WLHSV(DMO)=0.36 h^{-1}, T = 503 K, P = 15 bar) in DMO hydrogenation over Cu_{20}/SiO_2, Re_5Cu_5/SiO_2 and Re_5Cu_{20}/SiO_2 catalysts. 20% DMO in methanol was used in the feed.

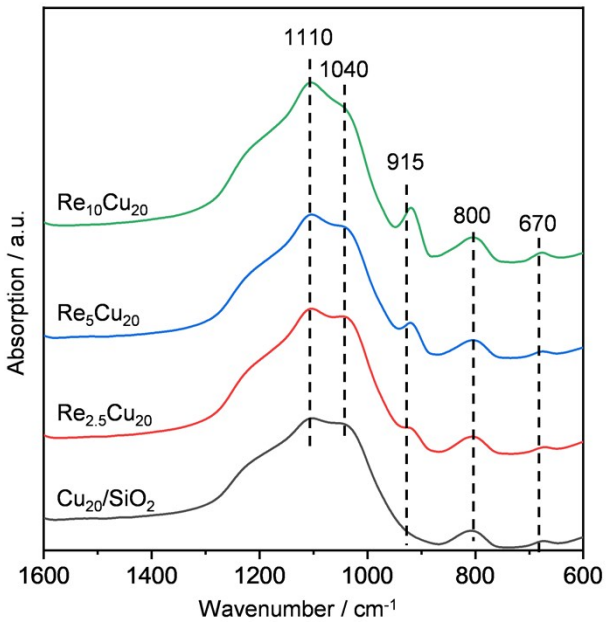

Fig. S3. FT-IR spectra of selected catalysts. The bands at 1110 and 800 cm^{-1} can be assigned to the $\nu_{Si\text{-}O}$ asymmetric and symmetric stretching vibrations, respectively; the bands at 1040 and 670 cm^{-1} are related to the $\delta_{O\text{-}H}$ of copper phyllosilicate, and the band at 915 cm^{-1} is characteristic of the Re-O bonds. The relative contribution of the copper phyllosilicate phase could be estimated by comparing the band intensity of I_{670}/I_{800}. This value only shows little changes upon Re addition (0.84-0.88) compared that of Cu_{20}/SiO_2 (0.88), suggesting the copper phyllosilicate phase is not much influenced by the dopants.

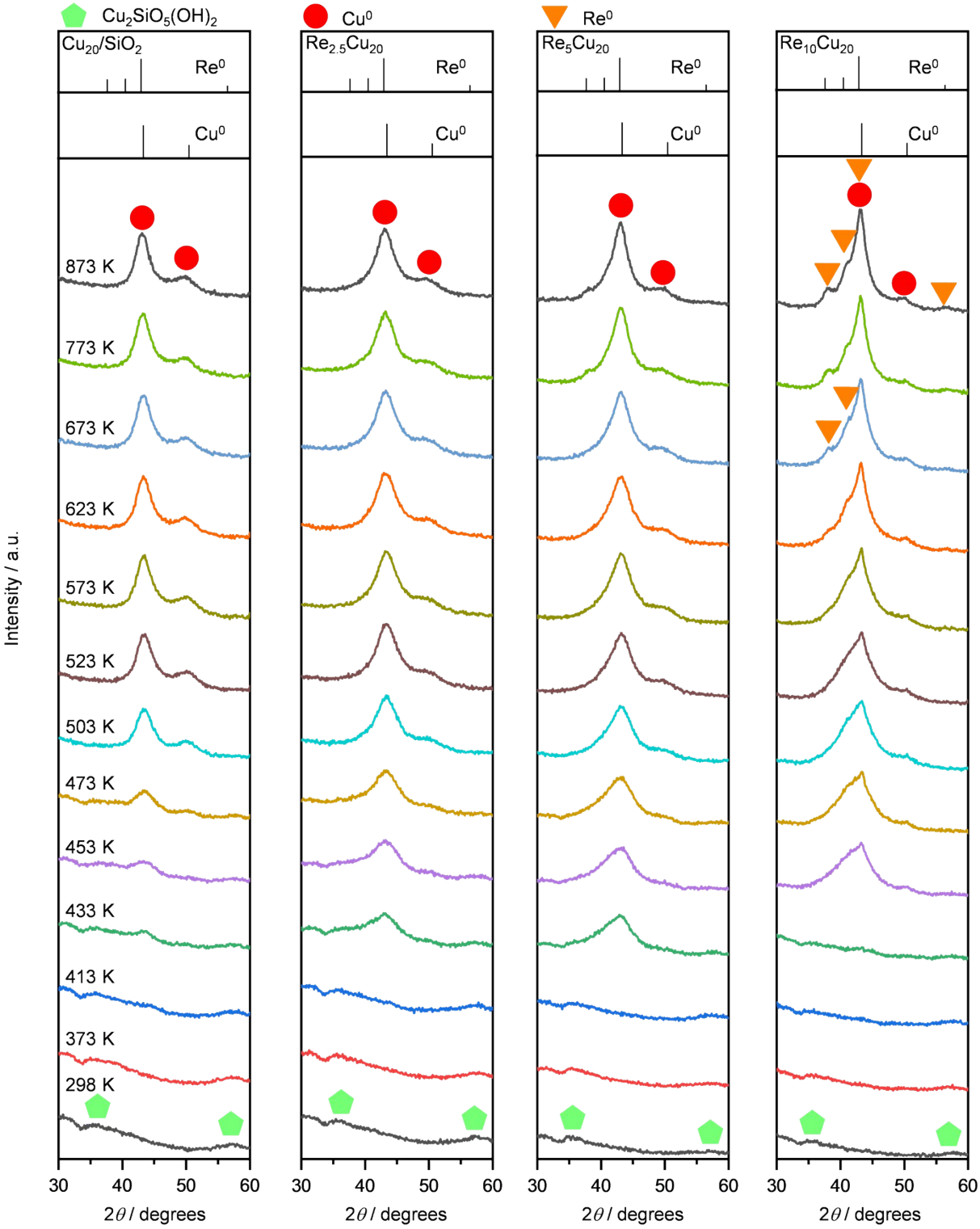

Fig. S4. *In situ* XRD patterns of selected catalysts recorded from 298 to 873 K under reductive ambience (H_2, flow rate: 30 cm^3 min^{-1}).

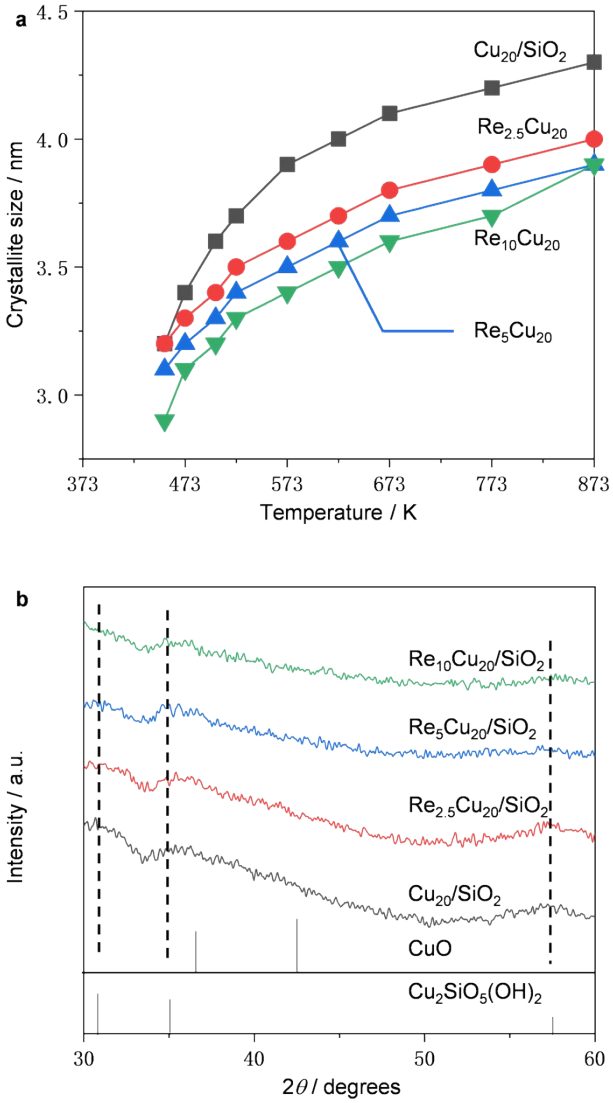

Fig. S5. a. The crystallite sizes of the key catalysts, estimated by Scherrer equation using the Cu (111) facet at 43.2° 2θ, as a function of the ramping temperature. **b**. XRD patterns of the selected catalysts after calcination recorded at 298 K.

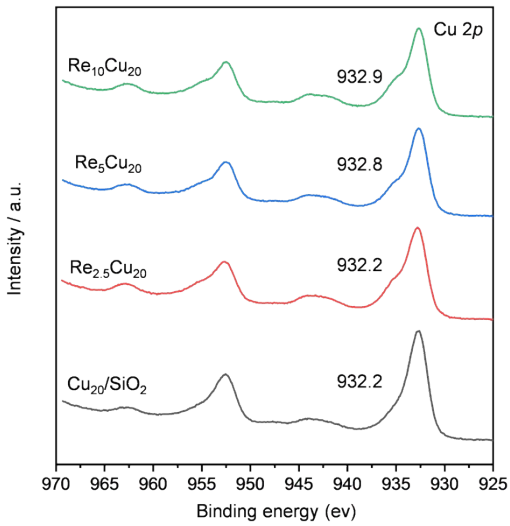

Fig. S6. Cu 2*p* XPS spectra of the key catalysts after *ex situ* H_2 reduction treatment (503 K, 4 h).

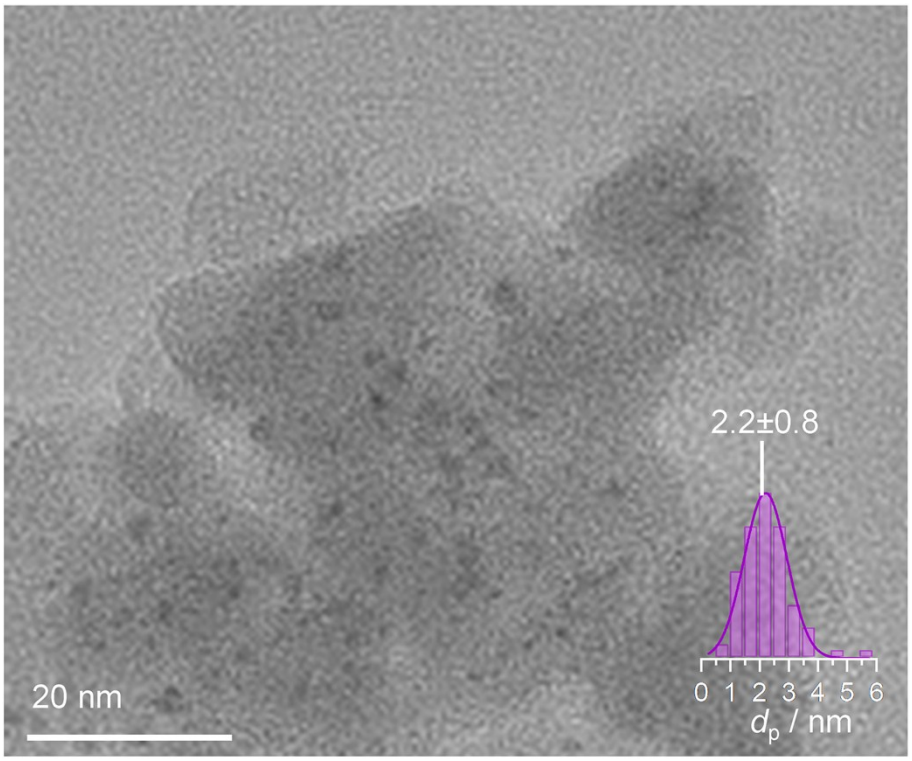

Fig. S7. TEM image of the Re_5Cu_5/SiO_2 catalyst after *ex situ* H_2 reduction treatment (503 K, 4 h), with pore size distribution (inset).

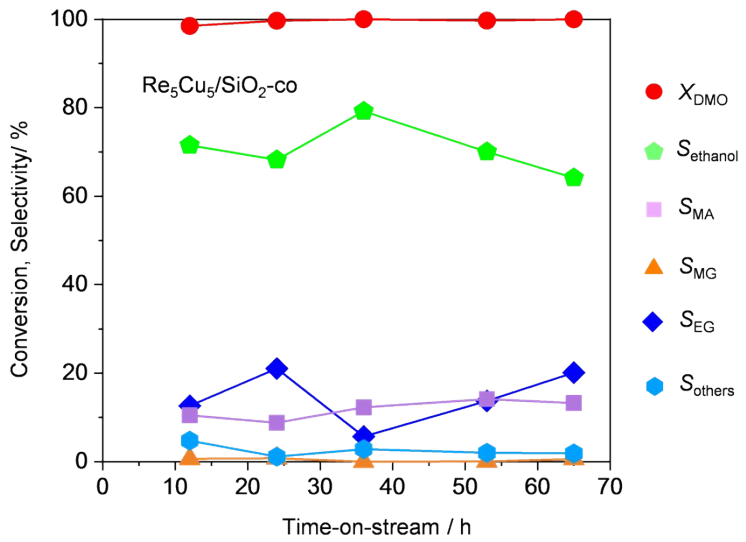

Fig. S8. Long-term stability performance of Re_5-Cu_5/SiO_2-co catalyst in DMO hydrogenation. Reaction conditions: WLHSV(DMO) = 0.36 h^{-1}, H_2/DMO=280, T = 503 K, and P = 15 bar. 20% DMO in methanol was used in the feed.

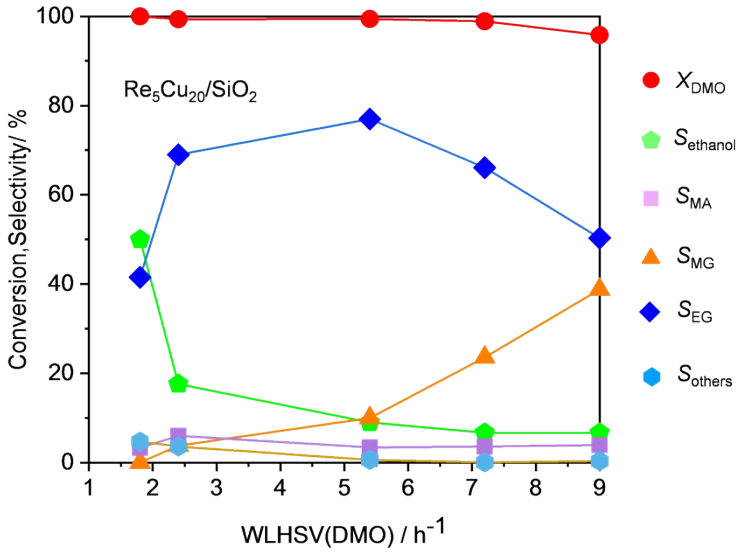

Fig. S9. The catalytic performance of Re_5-Cu_{20}/SiO_2 as a function of the WLHSV(DMO). Reaction conditions: H_2/DMO=70, T = 503 K, and P = 15 bar. 20% DMO in methanol was used in the feed.

Supplementary references

1. X. Wang, M. Chen, X. Chen, R. Lin, H. Zhu, C. Huang, W. Yang, Y. Tan, S. Wang, Z. Du, Y. Ding, *J. Catal*., 2020, **383**, 254-263.
2. Y. Liu, J. Ding, J. Sun, J. Zhang, J. Bi, K. Liu, F. Kong, H. Xiao, Y. Sun, J. Chen, *Chem. Commun*., 2016, **52**, 5030-5032.
3. Y. Liu, J. Ding, J. Bi, Y. Sun, J. Zhang, K. Liu, F. Kong, H. Xiao, J. Chen, *Appl. Catal. A*, 2017, **529**, 143-55.
4. J. He, Y. Zhao, Y. Wang, J. Wang, J. Zheng, H. Zhang, G. Zhou, C. Wang, S. Wang, X. Ma, *Chem. Commun*., 2017, **53**, 5376-5379.
5. X. Shang, H. Huang, Q. Han, Y. Xu, Y. Zhao, S. Wang, X. Ma, *Chem. Commun*., 2019, **55**, 5555-5558.
6. W. Guo, Q. Yin, L. Zhu, S. Wang, *Adv. Mater. Res*., 2012, **550-553**, 175-178.
7. S. Zhao, H. Yue, Y. Zhao, B. Wang, Y. Geng, J. Lv, S. Wang, J. Gong, X. Ma, *J. Catal*., 2013, **297**, 142-150.
8. P. Ai, M. Tan, P. Reubroycharoen, Y. Wang, X. Feng, G. Liu, G. Yang, N. Tsubaki, *Catal. Sci. Technol*., 2018, **8**, 6441-6451.
9. Y. Zhao, S. Zhao, Y. Geng, Y. Shen, H. Yue, J. Lv, S. Wang, X. Ma, *Catal. Today*, 2016, **276**, 28-35.
10. G. Shu, K. Ma, S. Tang, C. Liu, H. Yue, B. Liang, *Catal. Today*, 2019, DOI: 10.1016/j.cattod.2019.**12**.034.
11. M. Abbas, J. Zhang, Z. Chen, J. Chen, *New J. Chem*., 2018, **42**, 17553-17562.
12. P. Ai, M. Tan, N. Yamane, G. Liu, R. Fan, G. Yang, Y. Yoneyama, R. Yang, N. Tsubaki, *Chem. Euro. J*., 2017, **23**, 8252-8261.
13. Y. Zhu, Y. Zhu, G. Ding, S. Zhu, H. Zheng, Y. Li, *Appl. Catal. A*, 2013, **468**, 296-304.
14. Y. Zhu, X. Kong, S. Zhu, F. Dong, H. Zheng, Y. Zhu, Y. Li, *Appl. Catal. B*, 2015, **166-167**, 551-559.
15. J. Zhu, W. Sun, S. Wang, G. Zhao, Y. Liu, Y. Lu, *Chem. Commun*., 2019, DOI: 10.1039/c9cc07389b.
16. H. Yue, Y. Zhao, S. Zhao, B. Wang, X. Ma, J. Gong, *Nat. Commun*., 2013, **4**, 2339.
17. M. Abbas, Z. Chen, J. Chen, *J. Mater. Chem. A*, 2018, **6**, 19133-19142.
18. J. Ding, Y. Liu, J. Zhang, K. Liu, H. Xiao, F. Kong, Y. Sun and J. Chen, *Catal. Sci. Technol*., 2016, **6**, 7220-7230.
19. S. Yin, L. Zhu, X. Wang, Y. Liu, S. Wang, *Chin. J. Chem. Eng*., 2019, **27**, 386-90.
20. J. Zhu, G. Zhao, W. Sun, Q. Nie, S. Wang, Q. Xue, Y. Liu, Y. Lu, *Appl. Catal. B*, 2020, **270,** 118873.